HHS Public Access

Author manuscript

Cell Rep. Author manuscript; available in PMC 2020 March 19.

Published in final edited form as:

Cell Rep. 2019 July 16; 28(3): 605–615.e4. doi:10.1016/j.celrep.2019.06.050.

Projection from the Amygdala to the Thalamic Reticular Nucleus Amplifies Cortical Sound Responses

Mark Aizenberg[1], **Solymar Rolón-Martínez**[1], **Tuan Pham**[2], **Winnie Rao**[1], **Julie S. Haas**[2], **Maria N. Geffen**[1,3,*]

[1]Department of Otorhinolaryngology: HNS, Department of Neuroscience, University of Pennsylvania, Philadelphia, PA, USA

[2]Department of Biological Sciences, Lehigh University, Bethlehem, PA, USA

[3]Lead Contact

SUMMARY

Many forms of behavior require selective amplification of neuronal representations of relevant environmental signals. Emotional learning enhances sensory responses in the sensory cortex, yet the underlying circuits remain poorly understood. We identify a pathway between the basolateral amygdala (BLA), an emotional learning center in the mouse brain, and the inhibitory reticular nucleus of the thalamus (TRN). Optogenetic activation of BLA suppressed spontaneous, but not tone-evoked, activity in the auditory cortex (AC), amplifying tone-evoked responses. Viral tracing identified BLA projections terminating at TRN. Optogenetic activation of amygdala-TRN projections further amplified tone-evoked responses in the auditory thalamus and cortex. The results are explained by a computational model of the thalamocortical circuitry, in which activation of TRN by BLA primes thalamocortical neurons to relay relevant sensory input. This circuit mechanism shines a neural spotlight on behaviorally relevant signals and provides a potential target for the treatment of neuropsychological disorders.

Graphical Abstract

*Correspondence: mgeffen@pennmedicine.upenn.edu.

AUTHOR CONTRIBUTIONS

M.A. and M.N.G. designed the experiments; M.A. and S.R.-M. carried out the experiments; W.R. assisted with the experiments; T.P. and J.S.H. implemented the model; M.A., M.N.G., S.R.-M., T.P., and J.S.H. analyzed the data; and M.A., S.R.M., J.S.H., and M.N.G. wrote the paper.

SUPPLEMENTAL INFORMATION

Supplemental Information can be found online at https://doi.org/10.1016/j.celrep.2019.06.050.

DECLARATION OF INTERESTS

The authors declare no competing interests.

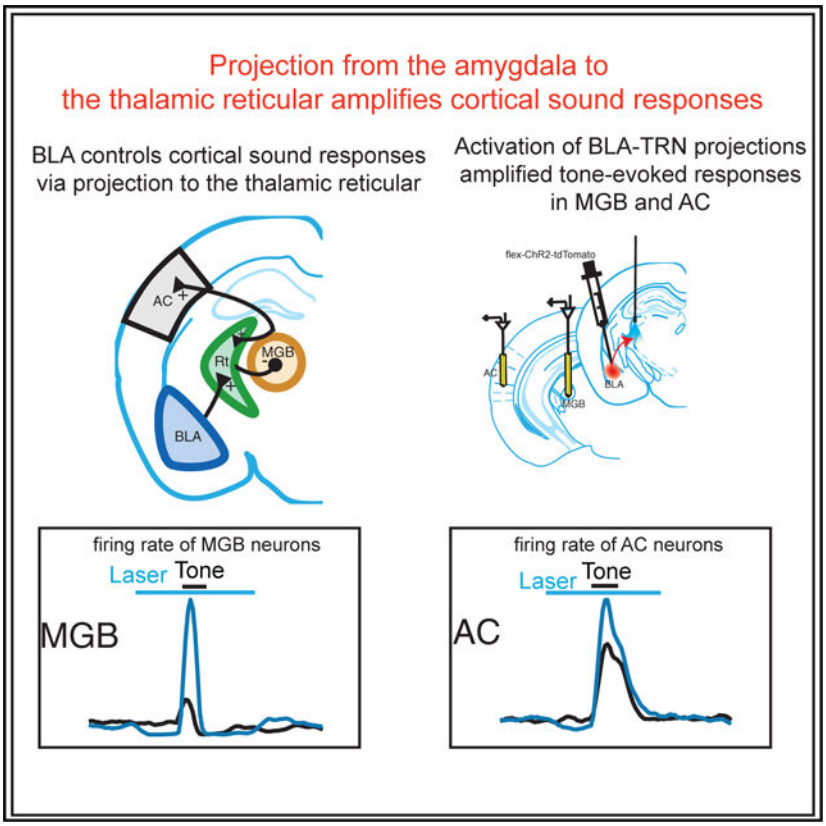

In Brief

Aizenberg et al. show that the projection from the emotional center of the brain, the basolateral amygdala, to the auditory thalamic control area, the thalamic reticular nucleus, gates sensory processing in the cortex.

INTRODUCTION

In our everyday experiences, we encounter the same sensory stimuli under different behavioral and emotional contexts, which can modify their behavioral relevance. If a stimulus is repeatedly encountered in an emotionally salient context, sensory resources are reallocated to preferentially encode that stimulus (Öhman et al., 2001; Phelps et al., 2006). This is particularly important for dangerous, fear-evoking stimuli. Behaviorally, the link between emotional learning, such as fear conditioning, and changes in sensory processing has been established in humans and other mammals. Recently, we found that differential fear conditioning can lead to an impairment or an improvement in sensory discrimination, depending on the generalization of learning, and that the auditory cortex is required for expression of these perceptual changes (Aizenberg et al., 2015). Similar effects were found following fear conditioning in humans (Li et al., 2008; Resnik and Paz, 2015; Resnik et al., 2011). Many neuropsychological disorders, including schizophrenia (Ferrarelli and Tononi, 2011; Young and Wimmer, 2017) and anxiety disorders (Öhman et al., 2001; Phillips et al., 2003), are characterized by inappropriate emotional weighting of sensory stimuli.

Untangling the mechanisms that govern emotion-driven control of sensory perception is important not only for basic understanding of sensory processing in everyday environments, but also for identifying potential treatment targets characterized by abnormal emotional responses to benign sensory stimuli.

The basolateral amygdala (BLA) is a critically important hub for the formation and expression of fear memories associated with sensory stimuli (for review, see LeDoux, 2000). Aversive stimuli drive strong responses in the BLA (Ghosh and Chattarji, 2015; Quirk et al., 1997; Resnik and Paz, 2015) (although they can be heterogeneous; Grewe et al., 2017), and fear conditioning evokes plastic changes in neuronal responses to conditioned sounds in the sensory cortex (Grosso et al., 2015; Kumar et al., 2012; Sacco and Sacchetti, 2010; Weinberger, 2004). The BLA has been proposed to drive plasticity in the auditory cortex (AC) for signals associated with fear (Li et al., 2008; Padmala and Pessoa, 2008). While changes in the AC following fear conditioning have been extensively documented (for review, see Weinberger, 2004), it is not clear whether and how the BLA modulates cortical responses to sensory stimuli (Chavez et al., 2009; Letzkus et al., 2011).

The lateral amygdala (LA) sends direct projections to the AC, as evidenced by imaging of LA axons in the AC (Yang et al., 2016). However, recent studies in the primate brain revealed an additional pathway from the BLA to the primary inhibitory nucleus in the thalamus, the thalamic reticular nucleus (TRN) (Zikopoulos and Barbas, 2012). This finding raises the possibility that the TRN facilitates the gating of signals in the sensory cortex from the BLA. The TRN is a layer of inhibitory gamma-aminobutyric acid (GABA)ergic neurons located between the neocortex and thalamus that does not send direct projections to the neocortex but provides inhibition for the sensory thalamocortical relay cells (Steriade et al., 1985). At the same time, the TRN receives excitatory collaterals from the cortex and thalamus (Pinault, 2004). These projections position the TRN as a gate-keeper, controlling sensory information flowing from the thalamus to the cortex and potentially suppressing irrelevant stimuli, offering an opportunity to reweigh sensory responses based on their behavioral saliency (Ahrens et al., 2015; Halassa et al., 2014; Wimmer et al., 2015).

Here, we first tested the effects of activation of the BLA on tone-evoked responses in the AC. We found that activating the BLA suppressed spontaneous activity in the AC, leading to an increase in tone-evoked response amplitude. By examining the connectivity between the BLA and the thalamus using viral anterograde and retrograde viral-tracing techniques in the mouse, we identified direct projections from the BLA to the TRN. We found that activating this connection selectively suppressed spontaneous activity in the auditory thalamus, similar to the effects of activating the BLA on the AC. Through a computational model of thalamocortical circuitry, we found that activating the BLA inputs to the TRN could account for the reduction in spontaneous thalamic activity, and this reduction acted to prime the thalamocortical relay response to sensory input. Together, these findings suggest that the amygdala-TRN pathway amplifies responses to sensory input by suppressing spontaneous activity of relay neurons, a process that could underlie fear-driven changes in auditory and other forms of sensory discrimination.

RESULTS

Photo-Activation of the BLA Amplifies Tone-Evoked Responses in the AC

We first tested the effect of optogenetic activation of the BLA on spontaneous and tone-evoked activity in the AC. To manipulate the level of activity of excitatory neurons in the amygdala, we expressed channelrhodopsin (ChR2) using targeted viral delivery to the BLA of mice expressing Cre recombinase in neurons under the CamKIIα promoter (CamKIIα-Cre mice, Figure 1A for data; for all figures here and below, see https://doi.org/10.6084/m9.figshare.8226329). Injection of a modified adeno-associated virus (AAV), which carried the antisense code for ChR2 under the FLEX cassette, resulted in efficient and specific expression of ChR2 (flex-ChR2) in excitatory neurons in the BLA of CamKIIα-Cre mice (Figure 1B).

We measured spontaneous and tone-evoked activity of neurons in the AC, targeting the primary AC (A1), by recording from awake, head-fixed mice during the acoustic presentation of a random tone sequence consisting of 50-ms tone pips at 50 frequencies, ranging from 1 to 80 kHz (70 dB SPL). The BLA was activated by shining a blue laser light (473 nm, 3.5 mW/mm^2 intensity at the fiber tip) through implanted optic cannulas. Photo-activation of the BLA significantly reduced the overall spontaneous firing rate (FR_{base}; computed during the baseline period, 0–50 ms prior to tone onset; N = 190, p = 8.15e-7, df = 189, tstat = 5.10) in the AC (Figures 1C, 1D, and 1G). While the peak tone-evoked firing rate in the AC (FR_{tone}; computed 0–50 ms after tone onset) was not significantly affected by the BLA activation (Figures 1C, 1D, and 1H; n.s.), the amplitude of responses to tones, compared with the spontaneous firing rate, increased (Figures 1D and 1I; N = 190, p = 2.12e-10, tstat = 6.72). Activation of the BLA did not significantly affect the tuning bandwidth of neurons in the AC, quantified by the sparseness of the tuning curve (Figures 1E, 1F, and 1J; n.s.). Thus, by reducing the spontaneous firing rate, but not increasing the tone-evoked response, activation of the BLA amplified the tone-evoked responses in the AC.

The BLA Sends Projections to the TRN

Suppression of the spontaneous firing in cortical neurons during BLA activation is most likely due to an inhibitory synapse. Recent studies identified direct projections from the BLA to the TRN, an inhibitory nucleus in the thalamus (Zikopoulos and Barbas, 2012). The TRN in turn projects to the medial geniculate body (MGB); therefore, activation of the BLA could drive the suppression of spontaneous activity in the AC by activating inhibitory TRN to MGB projections. We observed that the AAV injected in the BLA resulted in the labeling of projections in the TRN (Figure 1A). To confirm the existence of the BLA-TRN pathway, we injected retro adeno-associated virus (rAAV)-encoding GFP in the TRN, as well as a retrograde CAV2-Cre vector in the TRN of AI14 reporter mice, in which tdTomato is conditionally expressed in the cells transfected with Cre recombinase. We identified the retrograde labeling of neurons in the basolateral and central nuclei of the amygdala (Figures 2A and S1), confirming the existence of a direct pathway from the BLA to the TRN.

Photo-Activation of the BLA-TRN Pathway Increases the Amplitude of Tone-Evoked Responses in the AC

To test whether the BLA-TRN pathway underlies the amplification of tone-evoked responses caused by the BLA activation (Figure 1), we injected either a vector expressing hChR2 under the CAG promoter in the BLA of wild-type (WT) mice or a flex-ChR2 vector into the BLA of CamKIIα-Cre mice. We then shined a blue laser light onto the TRN through the implanted cannulas, while recording the neural responses in the AC using multichannel silicon probes (Figure 2B). This allowed us to test the effect of selective activation of neurons that project from the BLA to the TRN on neuronal activity in the AC. Activation of BLA terminals in the TRN led to a significant suppression of spontaneous neuronal activity in the AC (Figures 2C, 2D, and 2G; N = 216, p = 0.0067, df = 215, tstat = 2.74), whereas the absolute tone-evoked firing rate was significantly increased (Figures 2D and 2H; N = 216, p = 0.0048, df = 215, tstat = 2.85). Hence, the average amplitude of responses to the tones increased significantly (Figures 2D and 2I; N = 216, p = 5.0e–8, df = 215, tstat = 5.65). The sparseness of the tuning curves increased as a result of TRN activation (Figures 2E, 2F, and 2J; N = 216, p = 2.73e–10, df = 215, tstat = 6.62).

These effects persisted when we also blocked the activity of BLA neurons by the focal application of the tetrodotoxin (TTX) (Figures S2A–S2F; with TTX: N = 75, decrease in spontaneous activity, p = 3.03e–11, df = 74, tstat = 7.8; increase in response amplitude, p = 0.0061, df = 74, tstat = 2.82; Figures S2G and S2H; without TTX: N = 74, decrease in spontaneous activity, p = 1.49e 10, df = 73, tstat = 7.45; increase in response amplitude, p = 7.01e–6, df = 73, tstat = 4.84). This control ensured that our stimulation of the BLA-TRN terminals did not lead to the activation of another pathway originating from the cell bodies in the BLA (Jhang et al., 2018; Lerner et al., 2016; Znamenskiy and Zador, 2013). Combined, these results demonstrate that selective activation of the BLA-TRN projections evokes similar effects to those observed with general BLA activation on activity in the AC.

Photo-Activation of the BLA-TRN Pathway Increases the Amplitude of Tone-Evoked Responses in the Auditory Thalamus

There is extensive evidence that the TRN inhibits sensory processing in the sensory thalamus (Ahrens et al., 2015; Shosaku, 1986). Therefore, we hypothesized that the effect of the BLA-TRN pathway on the AC activity is the result of inhibition that the auditory thalamus receives from the TRN (Figure 3A, left). We tested whether the activation of the BLA-TRN terminals drives similar effects to those observed in the AC in the auditory thalamus (medial geniculate body [MGB]). We tested this hypothesis by optogenetically activating the BLA-TRN pathway as described above, while simultaneously recording from the MGB (Figures 3A and 3B). Similar to the previous results, the photo-activation of amygdalar terminals in the TRN led to a significant suppresion of the spontaneous firing rate of neurons in the MGB (Figures 3C and 3F; N = 126, p = 8.97e–10, df = 125, tstat = 6.63). In contrast, the mean tone-evoked activity was not affected by photo-stimulation (Figures 3C and 3G; n.s.), resulting in an increased amplitude of tone-evoked responses (Figure 3H; p = 9.6e–7, df = 125, tstat = 5.16). Similar to the AC recordings, photo-activation of the BLA-TRN pathway increased the sparseness of the tuning curve (Figures 3D, 3E, and 3I; p =

8.65e–5, df = 125, tstat = 4.06). Combined, our findings are consistent with the hypothesis that the BLA-TRN pathway acts on the AC through the MGB.

To verify that the effect of light on the activity in the auditory thalamus and cortex is specific to the action of the ChR2, we injected a control group of mice with a viral vector that encoded only fluorescent protein. In the control mice, shining blue light on the BLA projections in the TRN did not cause any significant changes in the firing rates of neurons, either in the AC (Figure S3) or the MGB (Figure S4).

A Bursting Model of the TRN and MGB Produces Enhancement in Tone-Evoked Responses in the TRN and A1 due to BLA-TRN Activation

Can the enhanced responsiveness to tones be compatible with the decreased spontaneous activity upon the BLA-TRN activation? These dual effects may be explained by the feedback connectivity between the bursting neurons in the TRN and MGB. We constructed a three-cell model of MGB, TRN, and AC neurons (Figure 4). As all thalamic neurons exhibit bursts of spikes resulting from T currents (Gribkova et al., 2018; Huguenard, 1996; Willis et al., 2015), we used a bursting neuron model for our TRN and MGB neurons (Haas and Landisman, 2012; Traub et al., 2005a). Our simulation code is available at https://github.com/jhaaslab/trn_aud. Spontaneous spiking was elicited by Poisson-distributed inputs to the MGB and AC neurons. We delivered a 100-ms-long pulse of input to the TRN neuron to represent the optogenetic activation of BLA terminals in the TRN, and a shorter 10-ms input to the MGB to represent the tone input. The BLA activation initiated a burst in the TRN neurons, with regular tonic firing following the burst for increased strengths of BLA activation (Figure 4B, first column). For weak BLA input, the initial burst in the TRN was late and elicited fewer spikes, providing only a weak inhibition of the spontaneous firing in the MGB and of the MGB response when the tone arrived (second row in Figures 4B and 4C). For moderate values of BLA activation, a quicker and stronger burst in the TRN delivered a stronger and earlier inhibition in the MGB and AC (third row in Figures 4B and 4C). This inhibition terminated the spontaneous firing in the MGB, and the timing of the TRN burst resulted in a stronger rebound from inhibition in the MGB neuron. Together, these effects allowed the MGB and AC to produce an amplified response when the tone arrived. Overactivation of the BLA (bottom row in Figures 4B and 4C) led to overactivation of the TRN and, correspondingly, stronger and more persistent inhibition of the MGB and AC. These effects of strength and timing of the TRN bursts on firing rates in the MGB and AC are summarized in Figure 4D. Consistent with the experimental results, the suppression of spontaneous MGB spiking allowed for an increased ability to respond to the auditory input and relay it to the AC. Together, these results provide a link between the suppression of spontaneous activity and the amplified AC response by demonstrating that a moderate activation by the BLA of the TRN, such as those used in our experiments, increases the readiness of the MGB neurons to respond. As a result, the peak-to-peak firing rates in the MGB and AC increased during the BLA activation (Figure 4E).

DISCUSSION

The BLA is an important brain area for auditory fear conditioning (for review, see LeDoux, 2000), where conditioned and unconditioned stimuli converge (Romanski et al., 1993; Romanski and LeDoux, 1992). Lesions of the BLA (Campeau and Davis, 1995; Goosens and Maren, 2001), or of either the lemniscal or nonlemniscal auditory inputs to the BLA, impair the acquisition, expression, and discrimination of conditioned fear responses (Antunes and Moita, 2010; Boatman and Kim, 2006), whereas paired activation of the BLA with an auditory cue is sufficient to induce a conditioned fear response (Johansen et al., 2010). Recent studies found that sensory fear conditioning can modulate sensory discrimination acuity (Li et al., 2008; Resnik et al., 2011), and we demonstrated that in the auditory system, this modulation requires the AC (Aizenberg and Geffen, 2013). Therefore, in the present study, we examined whether and how activating the BLA affects tone-evoked responses in the AC. We first found that activating the BLA increases the tone-evoked response amplitude in the AC by suppressing spontaneous activity, but not affecting tone-evoked responses. We identified a mechanism by which this suppression can occur—via the projections from the BLA to the inhibitory nucleus of the thalamus, the TRN. Consistent with established anatomy, we did not find significant direct projections from the TRN to the AC. Therefore, we hypothesized that the TRN controls responses in the AC via the MGB of the auditory thalamus (Kimura et al., 2007). Indeed, specifically activating the BLA-TRN projection neurons drove an increase in the tone-evoked response amplitude in both the MGB and the AC. The effects were stronger in the MGB than the AC, further suggesting that the MGB serves as a relay for cortico-collicular control. These effects could be accounted for by a three-cell model of the TRN-MGB-AC connections (Figures 3A and 4), with the critical effect provided by the difference in timing and magnitude of the inhibition that the TRN delivered to the MGB, consistent with previous thalamocortical models (Gribkova et al., 2018; Haas and Landisman, 2012; Pham and Haas, 2018; Willis et al., 2015). Our study thus establishes an important pathway connecting the emotional and sensory processing centers that potentially drives changes in auditory perception as a result of emotional learning.

The TRN is a thin sheet of GABAergic neurons surrounding the dorsal thalamus, which exhibits sectorial anatomical organization, such that each sector of the TRN is specific to a sensory modality (Guillery et al., 1998; Jones, 1975). Although the TRN does not send direct projections to the sensory cortical areas, it can control the flow of auditory and other sensory information to the cortex by inhibiting or disinhibiting thalamic projection neurons (Kimura et al., 2007, 2012; Pinault and Deschênes, 1998; Villa, 1990). The unique anatomical and functional organization of the TRN gave rise to the “attentional searchlight” hypothesis (Crick, 1984), which proposed that the TRN drives attention toward salient stimuli by inhibiting sensory responses to irrelevant information. Our results imply that the BLA is one of the controls of that searchlight, control that is exerted by inhibiting spontaneous activity in the relay cells. Our parameters also suggest that fear-driven BLA activation that is too weak, or conversely, overwhelming, fails to control the spotlight. We suggest that this simple mechanism may apply to multiple arising senses as they pass through the thalamocortical circuit.

Communication across the TRN (Landisman et al., 2002) or by convergence and divergence of TRN-thalamic connections offers the possibility for the activation of one specific sense, or sensory modality, to affect the thalamic relay of another sense (Brown et al., 2019; Willis et al., 2015). Recently, the TRN was experimentally shown to selectively amplify the processing of task-relevant stimuli and attention-guided behaviors. Either genetic (knockout or knockdown of the ErbB4 receptor in TRN neurons) or optogenetic perturbation of neuronal activity in the TRN diminished attentional switching between conflicting sensory cues in a two-alternative-choice task (Ahrens et al., 2015; Wimmer et al., 2015). Similarly, optogenetic activation of the TRN during the window of elevated attention to a visual cue interfered with the performance in a visual-detection task (Halassa et al., 2014). Our present results showing that TRN activity is modulated by its inputs from the BLA suggest that emotional responses generated in the amygdala may also modulate sensory interactions within and through the TRN, particularly during fear learning.

Auditory fear conditioning drives plastic changes to tone-evoked responses in the auditory thalamus (Lennartz and Weinberger, 1992) and AC (Weinberger, 2004; Weinberger et al., 1993). Multineuronal recording in the AC demonstrated that tone-evoked responses to the conditioned stimulus are increased following fear conditioning (Bakin and Weinberger, 1990), with individual neurons exhibiting heterogeneous but sustained changes in their tuning properties (Weinberger et al., 1993). Auditory fear conditioning promotes the formation of dendritic spines in the AC (Moczulska et al., 2013), pointing to plastic changes in neuronal connectivity. Direct amygdala-cortical projections are thought to underlie the facilitation of responses to emotionally salient stimuli (Amaral and Price, 1984; Yang et al., 2016; Yukie, 2002), as fear conditioning leads to an increase in the post-synaptic spines and pre-synaptic boutons specific to BLA-AC neuronal pairs (Yang et al., 2016). Here, we demonstrate a parallel processing pathway to the cortex from the BLA via the TRN and MGB (Figure 3A). This pathway may potentially play a regulatory role during the acquisition and recall of auditory fear memories. These two pathways may complement each other in enhancing responses to the conditioned stimulus by strengthening the amygdala-cortical connectivity. In future studies, it will be important to account for the interactions between these pathways in interpreting the effects of fear conditioning and learning on sensory responses in the cortex.

We previously found that generalized auditory fear learning led to an impairment in frequency discrimination acuity, whereas specialized learning led to an improvement in acuity (Aizenberg and Geffen, 2013). Similar bi-directional changes in auditory discrimination were achieved by manipulating the activity of inhibitory interneurons in the cortex (Aizenberg et al., 2015). The existence of parallel pathways for controlling tone-evoked responses after activation of the BLA may be useful for enabling bi-directional changes in sensory processing. In particular, top-down control of inhibition early in sensory processing is useful in gating incoming sensory information. The connection that we identified here may be a manifestation of a more general principle of control of behavioral performance via inhibitory-excitatory interactions (Wood et al., 2017).

STAR★METHODS

LEAD CONTACT AND MATERIAL AVAILABILITY

Further information and requests for resources and reagents should be directed to and will be fulfilled by the Lead Contact, Maria Geffen (mgeffen@pennmedicine.upenn.edu).

EXPERIMENTAL MODEL AND SUBJECT DETAILS

All experiments were performed in adult female (n = 5) or male (n = 14) mice (supplier: Jackson Laboratories) between 7–15 weeks of age weighing between 17–27 g. Strains: CamKIIα-Cre: B6.Cg-Tg(CamKIIα-Cre)T29–1Stl/J; wild-type mice: C57BL/6J), AI14: Rosa-CAG-LSL-tdTomato-WPRE::deltaNeo housed at 28°C on a 12 h light – dark cycle with water and food provided *ad libitum*, with fewer than five animals per cage. In CamKIIα-Cre mice, Cre was expressed in excitatory neurons. All animal work was conducted according to the guidelines of University of Pennsylvania IACUC and the AALAC Guide on Animal Research. Anesthesia by isoflurane and euthanasia by carbon dioxide were used. All means were taken to minimize the pain or discomfort of the animals during and following the experiments.

METHOD DETAILS

Surgery and Virus Injection—At least 10 days prior to the start of experiments, mice were anesthetized with isoflurane to a surgical plane. The head was secured in a stereotactic holder. For recordings targeting AC, the mouse was subjected to a small craniotomy (2 × 2 mm) over left AC under aseptic conditions (coordinates relative to Bregma: −2.6 mm anterior, 4.2 mm lateral, +1 mm ventral). For recordings targeting MGB, the mouse was subjected to a small craniotomy (0.5 × 0.5 mm) over left MGB (coordinates relative to Bregma: −3.2 mm anterior, 2.0 mm lateral). For optogenetic activation of BLA neurons, a small craniotomy (0.5 × 0.5 mm) was performed bilaterally over amygdala (coordinates relative to Bregma: 1.5 mm posterior, ± 3.0 mm lateral). Fiber-optic cannulas (Thorlabs, Ø200 μm Core, 0.39 NA) were implanted bilaterally over the craniotomy at depth of 4.4 mm from Bregma. For optogenetic activation of BLA projections to TRN, a small craniotomy (0.5 × 0.5 mm) was performed bilaterally over TRN (coordinates relative to Bregma: −1.1 mm anterior, ± 2.0 mm lateral). Fiber-optic cannulas were implanted bilaterally at depth of 2.7 mm from Bregma. Viral constructs were injected using a syringe pump (Pump 11 Elite, Harvard Apparatus) either in BLA (200–400 nl, 4.6 mm depth from Bregma) or in TRN (200 nl, 3.4 mm depth from Bregma). Craniotomies were covered with a removable silicon plug. A small headpost was secured to the skull with dental cement (C&B Metabond) and acrylic (Lang Dental).

For postoperative analgesia, Buprenex (0.1 mg/kg) was injected intraperitonially and lidocaine was applied topically to the surgical site. An antibiotic (0.3% Gentamicin sulfate) was applied daily (for 4 days) to the surgical site during recovery. Virus spread was confirmed postmortem by visualization of fluorescent protein expression in fixed brain slices, and its co-localization with excitatory neurons, following immuno-histochemical processing with the anti-CAMKIIα antibody.

Viral Vectors—Modified AAV vectors were obtained from Penn VectorCore. Modified AAV encoding ChR2 under FLEX promoter (Addgene: 18917-AAV9 AAV9-FLEX-ChR2-tdTomato) was used for activation of excitatory neurons in CamKIIα-Cre mice. hChR2 was used for activation of neurons in WT mice (Addgene: 100054-AAV5 AAV5-CAG-hChR2(H134R)-mCherry-WPRE-SV40). Modified AAV vectors encoding only tdTomato under a FLEX cassette were used as a control for the specific action of ChR2 on the neuronal populations. Cav2-cre virus (Viral Vector Production Unit) was used for retrograde tracing of BLA-TRN projections in AI24 mice that express tdTomato under FLEX cassette.

Histology—Brains were extracted following perfusion of 0.01 M phosphate buffer pH 7.4 (PBS) and 4% paraformaldehyde (PFA), postfixed in PFA overnight and cryoprotected in 30% sucrose. Free-floating coronal sections (40 μm) were cut using a cryostat (Leica CM1860). Sections were washed in PBS containing 0.1% Triton X-100 (PBST; 3 washes, 5 min), incubated at room temperature in blocking solution (10% normal goat serum and 0.2% bovine serum albumin in PBST; 1h), and then incubated in primary antibody diluted in carrier solution (1% normal goat serum and 0.2% bovine serum albumin in PBST) overnight at 4°C. Anti-CAMKIIα antibody was used to stain excitatory neurons (abcam5683 rabbit polyclonal, 1:500, abcam). The following day sections were washed in PBST (3 washes, 5 min), incubated for 2 hours at room temperature with secondary antibodies (Alexa 488 goat anti-rabbit IgG; 1:750), and then washed in PBST (4 washes, 10 min). Sections were mounted using fluoromount-G (Southern Biotech) and confocal or fluorescent images were acquired (Leica SP5 or Olympus BX43)

Photostimulation of Neuronal Activity—Neurons were stimulated by application of five 25 ms-long light pulses (25 ms inter-pulse interval) of blue laser light (473 nm, BL473T3–150, used for ChR2 stimulation), delivered through implanted cannulas. Timing of the light pulse was controlled with microsecond precision via a custom control shutter system, synchronized to the acoustic stimulus delivery. Prior to the start of the experiment, the intensity of the blue laser was adjusted to 3.5 mW/mm^2 as measured at the tip of the optic fiber.

Electrophysiological Recordings—All recordings were carried out as previously described (Aizenberg et al., 2015) inside a double-walled acoustic isolation booth (Industrial Acoustics). Mice were placed in the recording chamber, and their headpost was secured to a custom base, immobilizing the head. Activity of neurons was recorded either via a 32-channel silicon multi-channel probe (Neuronexus), or custom-made Microdrive housing multiple tetrodes lowered into the targeted area via a stereotactic instrument following a durotomy. Electro-physiological data were filtered between 600 and 6000 Hz (spike responses), digitized at 32kHz and stored for offline analysis (Neuralynx). Spikes belonging to single neurons were sorted using commercial software (Plexon).

Acoustic Stimulus—Stimulus was delivered via a magnetic speaker (Tucker-Davis Technologies), calibrated with a Bruel and Kjaer microphone at the point of the subject's ear, at frequencies between 1 and 80 kHz to ± 3 dB. To measure the frequency tuning curves, we presented a train of 50 pure tones of frequencies spaced logarithmically between 1 and

80 kHz, at 70 dB, each tone repeated twice in pseudo-random sequence, counter-balanced for laser presentation. The full stimulus was repeated 5 times. Each tone was 50 ms long, with inter-stimulus interval (ISI) of 450 ms. Laser stimulation occurred during every other tone, with an onset 100 ms prior to tone onset. Laser stimulation on each trial consisted of five 25 ms-long pulses with 25 ms-long inter-pulse intervals.

QUANTIFICATION AND STATISTICAL ANALYSIS

Neuronal Response Analysis—The spontaneous firing rate (FR_{base}) was computed from the average firing rate 50 ms before tone onset for light-On and light-Off trials. The tone-evoked firing rate (FR_{tone}) was computed as the average firing rate from 0 to 50ms after tone onset. To examine frequency selectivity of neurons, sparseness of frequency tuning was computed as:

$$Sparseness = 1 - \frac{\left(\sum_{i=1}^{i=n} FR_i/n\right)^2}{\sum_{i=1}^{i=n} FR_i^2/n}$$

where FR_i is tone-evoked response to tone at frequency i, and n is number of frequencies used.

The amplitude of neuronal response to tones was defined as the difference between mean spontaneous (0–50 ms before tone onset) and tone-evoked (0–50 ms after tone onset) firing rate and, for each neuron. Only responses to tones within 0.5 octaves of best frequency (the frequency which resulted in maximum firing rate) of each neuron were included.

Statistical Analysis—Data were analyzed using two-tailed paired t tests in MATLAB (Mathworks) following the Shapiro-Wilk test for normality. For all tests, the significance was assayed at $p < 0.05$. We compared the firing rates of neurons, computed as described above, on trials with and without laser stimulation, before (spontaneous, −50–0 ms) and after (tone-evoked, 0–50 ms) tone onset; as well as sparseness. The sample size (N = number of neurons), and statistical test results, such as *p*, *dstat* and *df* are reported in results for all measurements. Confidence intervals (standard error) are displayed in figures where appropriate.

Modeling—We used single-compartment Hodgkin-Huxley neuron models to create a 3-cell network consisting of a thalamic reticular nucleus (TRN) neuron, a thalamocortical neuron representing the MGB and a regular spiking neuron representing primary auditory cortex (AC; Figure 4A). Starting from the mechanistic models of Traub et al. (2005a, b) and Haas and Landisman (2012), we tuned cells with the following characteristics ($\bar{g}_X$ are maximal conductances with units of $[mS{=}cm^2]$ and E_X are reversal potentials in $[mV]$). We used the NEURON implementation in ModelDB (Traub et al., 2003, 2005b), accession numbers 20756, 45539. Our simulation code is available at https://github.com/jhaaslab/trn_aud.

	$\bar{g}_L$	$\bar{g}_{Naf}$	$\bar{g}_{Kdr}$	$\bar{g}_{KA}$	$\bar{g}_{K2}$	$\bar{g}_{CaT}$	$\bar{g}_{AR}$	E_K	E_L	E_{NA}	E_{Ca}	E_{AR}
TRN	0.1	60.5	60	5	0.5	0.75	0.025	−100	−75	50	125	−40
TC	0.04	100	33.75	6	2	0.75	0.25	−95	−70	50	125	−35
RS	0.04	200	170	20	0.5	0.1	0.1	−95	−70	50	125	−35

Chemical synapses included fast inhibitory $GABA_A$ ($E_{GABAR} = -80\ mV$) and excitatory AMPA ($E_{AMPAR} = 0\ mV$) synapses, both with NEURON implementation of AMPA point process synapses, in which the postsynaptic potentials consist of both rise time and fall times, with the former being 0.999 of the latter (*cf.* ModelDB accession number 45539). In our simulated network, MGB sent a feedforward excitatory AMPA synapse to TRN with $\tau_{AMPAR}^{TC \to TRN} = 2.0\ ms$ and $\bar{g}_{AMPAR}^{TC \to TRN} = 0.025\ \mu S$. The TRN neuron sent feedback inhibition via a $GABA_A$ synapse to the MGB neuron, with both fast and slow fall times (3.3ms and 10ms respectively [Traub et al., 2005a]) each contributing equally to the $GABA_A$ conductance $\bar{g}_{GABAR}^{TRN \to TC} = 0.050\ \mu S$. Finally, MGB also sent an AMPA synapse to AC with $\tau_{AMPAR}^{TC \to RS} = 2.0\ ms$ and $\bar{g}_{AMPAR}^{TC \to RS} = 0.20\ \mu S$. We set the synaptic delay to be 2:0 ms and the event detection threshold to be 25 mV

We simulated the network in NEURON for 600 ms, with $dt = 0{:}005 ms$; $V_0 = -60 mV$ and saved sampled data for visualization (Figure 4B) with sampling rate of $0{:}1 ms$. To simulate spontaneous activity in MGB, we added AMPA synapses with Poisson inputs, where $\tau_{AMPAR}^{Poisson} = 1.0\ ms$ and $\bar{g}_{AMPAR}^{Poisson} = 0.50\ \mu S$, to MGB at 50 Hz, to AC at 20 Hz and to TRN at 1 Hz. We used holding current to MGB at 1nA and to AC at 0.5nA.

We ran one simulation without any Poisson inputs (Figure 4B1) and 50 simulations for each condition with random Poisson inputs (Figures 4B2, 4B3, and 4C). In all simulations, we delivered a DC input of 10nA to MGB representing the tone inputs. We delivered a 100-ms input to TRN to represent BLA activation, at three strengths (0 nA, 0.5 nA, 0.8 nA, and 1.8 nA).

To quantify the results of simulations, we calculated the histograms of spike times, binned at 1 ms, then smoothed with a Hanning window of size 31. We normalized each rate to the maximum rate in the control condition preceding input to TRN. To calculate peak activity, we obtained the raw peak activity in the windows of tone input to MGB input for MGB and AC, then normalized those values to the control conditions. Peak-peak amplitude was taken as the difference between the raw peak activity during the tone and the mean activity during the 50 ms before the tone, also normalized to the control condition.

DATA AND CODE AVAILABILITY

The MATLAB .fig files with metadata are available at figshare: https://doi.org/10.6084/m9.figshare.8226329. The code for the model is available at github: https://github.com/jhaaslab/trn_aud.

Supplementary Material

Refer to Web version on PubMed Central for supplementary material.

ACKNOWLEDGMENTS

This work was supported by the National Institutes of Health (grants NIH R03DC013660, NIH R01DC014479, and NIH R01DC015527), the Klingenstein Award in Neuroscience, the Human Frontier in Science Foundation Young Investigator Award, and the Pennsylvania Lions Club Hearing Research Fellowship to M.N.G. and the National Science Foundation (NSF IOS 1557474) to J.S.H. M.N.G. is the recipient of the Burroughs Wellcome Award at the Scientific Interface. We thank the members of the Geffen Laboratory and the Hearing Research Center at the University of Pennsylvania, including Dr. Steve Eliades and Dr. Yale Cohen for comments and discussions.

REFERENCES

Ahrens S, Jaramillo S, Yu K, Ghosh S, Hwang G-RR, Paik R, Lai C, He M, Huang ZJ, and Li B (2015). ErbB4 regulation of a thalamic reticular nucleus circuit for sensory selection. Nat. Neurosci 18, 104–111. [PubMed: 25501036]

Aizenberg M, and Geffen MN (2013). Bidirectional effects of aversive learning on perceptual acuity are mediated by the sensory cortex. Nat. Neurosci 16, 994–996. [PubMed: 23817548]

Aizenberg M, Mwilambwe-Tshilobo L, Briguglio JJ, Natan RG, and Geffen MN (2015). Bidirectional Regulation of Innate and Learned Behaviors That Rely on Frequency Discrimination by Cortical Inhibitory Neurons. PLoS Biol. 13, e1002308. [PubMed: 26629746]

Amaral DG, and Price JL (1984). Amygdalo-cortical projections in the monkey (Macaca fascicularis). J. Comp. Neurol 230, 465–496. [PubMed: 6520247]

Antunes R, and Moita MA (2010). Discriminative auditory fear learning requires both tuned and nontuned auditory pathways to the amygdala. J. Neurosci 30, 9782–9787. [PubMed: 20660260]

Bakin JS, and Weinberger NM (1990). Classical conditioning induces CS-specific receptive field plasticity in the auditory cortex of the guinea pig. Brain Res. 536, 271–286. [PubMed: 2085753]

Boatman JA, and Kim JJ (2006). A thalamo-cortico-amygdala pathway mediates auditory fear conditioning in the intact brain. Eur. J. Neurosci 24, 894–900. [PubMed: 16930417]

Brown JW, Taheri A, Kenyon RV, Berger-Wolf T, and Llano DA (2019). A computational model of intrathalamic signaling via open-loop thalamo-reticular-thalamic architectures. bioRxiv. 10.1101/574178.

Campeau S, and Davis M (1995). Involvement of the central nucleus and basolateral complex of the amygdala in fear conditioning measured with fear-potentiated startle in rats trained concurrently with auditory and visual conditioned stimuli. J. Neurosci 15, 2301–2311. [PubMed: 7891168]

Chavez CM, McGaugh JL, and Weinberger NM (2009). The basolateral amygdala modulates specific sensory memory representations in the cerebral cortex. Neurobiol. Learn. Mem 91, 382–392. [PubMed: 19028592]

Crick F (1984). Function of the thalamic reticular complex: the searchlight hypothesis. Proc. Natl. Acad. Sci. USA 81, 4586–4590. [PubMed: 6589612]

Ferrarelli F, and Tononi G (2011). The thalamic reticular nucleus and schizophrenia. Schizophr. Bull 37, 306–315. [PubMed: 21131368]

Ghosh S, and Chattarji S (2015). Neuronal encoding of the switch from specific to generalized fear. Nat. Neurosci 18, 112–120. [PubMed: 25436666]

Goosens KA, and Maren S (2001). Contextual and auditory fear conditioning are mediated by the lateral, basal, and central amygdaloid nuclei in rats. Learn. Mem 8, 148–155. [PubMed: 11390634]

Grewe BF, Gründemann J, Kitch LJ, Lecoq JA, Parker JG, Marshall JD, Larkin MC, Jercog PE, Grenier F, Li JZ, et al. (2017). Neural ensemble dynamics underlying a long-term associative memory. Nature 543, 670–675. [PubMed: 28329757]

Gribkova ED, Ibrahim BA, and Llano DA (2018). A novel mutual information estimator to measure spike train correlations in a model thalamocortical network. J. Neurophysiol 120, 2730–2744. [PubMed: 30183459]

Grosso A, Cambiaghi M, Concina G, Sacco T, and Sacchetti B (2015). Auditory cortex involvement in emotional learning and memory. Neuroscience 299, 45–55. [PubMed: 25943482]

Guillery RW, Feig SL, and Lozsádi DA (1998). Paying attention to the thalamic reticular nucleus. Trends Neurosci. 21, 28–32. [PubMed: 9464683]

Haas JS, and Landisman CE (2012). State-dependent modulation of gap junction signaling by the persistent sodium current. Front. Cell. Neurosci 5, 31. [PubMed: 22319469]

Halassa MM, Chen Z, Wimmer RD, Brunetti PM, Zhao S, Zikopoulos B, Wang F, Brown EN, and Wilson MA (2014). State-dependent architecture of thalamic reticular subnetworks. Cell 158, 808–821. [PubMed: 25126786]

Huguenard JR (1996). Low-threshold calcium currents in central nervous system neurons. Annu. Rev. Physiol 58, 329–348. [PubMed: 8815798]

Jhang J, Lee H, Kang MS, Lee HS, Park H, and Han JH (2018). Anterior cingulate cortex and its input to the basolateral amygdala control innate fear response. Nat. Commun 9, 2744. [PubMed: 30013065]

Johansen JP, Hamanaka H, Monfils MH, Behnia R, Deisseroth K, Blair HT, and LeDoux JE (2010). Optical activation of lateral amygdala pyramidal cells instructs associative fear learning. Proc. Natl. Acad. Sci. USA 107, 12692–12697. [PubMed: 20615999]

Jones EG (1975). Some aspects of the organization of the thalamic reticular complex. J. Comp. Neurol 162, 285–308. [PubMed: 1150923]

Kimura A, Imbe H, Donishi T, and Tamai Y (2007). Axonal projections of single auditory neurons in the thalamic reticular nucleus: implications for tonotopy-related gating function and cross-modal modulation. Eur. J. Neurosci 26, 3524–3535. [PubMed: 18052989]

Kimura A, Yokoi I, Imbe H, Donishi T, and Kaneoke Y (2012). Auditory thalamic reticular nucleus of the rat: anatomical nodes for modulation of auditory and cross-modal sensory processing in the loop connectivity between the cortex and thalamus. J. Comp. Neurol 520, 1457–1480. [PubMed: 22101990]

Kumar S, von Kriegstein K, Friston K, and Griffiths TD (2012). Features versus feelings: dissociable representations of the acoustic features and valence of aversive sounds. J. Neurosci 32, 14184–14192. [PubMed: 23055488]

Landisman CE, Long MA, Beierlein M, Deans MR, Paul DL, and Connors BW (2002). Electrical synapses in the thalamic reticular nucleus. J. Neurosci 22, 1002–1009. [PubMed: 11826128]

LeDoux JE (2000). Emotion circuits in the brain. Annu. Rev. Neurosci 23, 155–184. [PubMed: 10845062]

Lennartz RC, and Weinberger NM (1992). Frequency-Specific Receptive Field Plasticity in the Medial Geniculate Body Induced by Pavlovian Fear Conditioning Is Expressed in the Anesthetized Brain. Behav. Neurosci 106, 484–497. [PubMed: 1616615]

Lerner TN, Ye L, and Deisseroth K (2016). Communication in Neural Circuits: Tools, Opportunities, and Challenges. Cell 164, 1136–1150. [PubMed: 26967281]

Letzkus JJ, Wolff SB, Meyer EMM, Tovote P, Courtin J, Herry C, and Lüthi A (2011). A disinhibitory microcircuit for associative fear learning in the auditory cortex. Nature 480, 331–335. [PubMed: 22158104]

Li W, Howard JD, Parrish TB, and Gottfried JA (2008). Aversive learning enhances perceptual and cortical discrimination of indiscriminable odor cues. Science 319, 1842–1845. [PubMed: 18369149]

Moczulska KE, Tinter-Thiede J, Peter M, Ushakova L, Wernle T, Bathellier B, and Rumpel S (2013). Dynamics of dendritic spines in the mouse auditory cortex during memory formation and memory recall. Proc. Natl. Acad. Sci. USA 110, 18315–18320. [PubMed: 24151334]

Öhman A, Flykt A, and Esteves F (2001). Emotion drives attention: detecting the snake in the grass. J. Exp. Psychol. Gen 130, 466–478. [PubMed: 11561921]

Padmala S, and Pessoa L (2008). Affective learning enhances visual detection and responses in primary visual cortex. J. Neurosci 28, 6202–6210. [PubMed: 18550762]

Pham T, and Haas JS (2018). Electrical synapses between inhibitory neurons shape the responses of principal neurons to transient inputs in the thalamus: a modeling study. Sci. Rep 8, 7763. [PubMed: 29773817]

Phelps EA, Ling S, and Carrasco M (2006). Emotion facilitates perception and potentiates the perceptual benefits of attention. Psychol. Sci 17, 292–299. [PubMed: 16623685]

Phillips ML, Drevets WC, Rauch SL, and Lane R (2003). Neurobiology of emotion perception II: Implications for major psychiatric disorders. Biol. Psychiatry 54, 515–528. [PubMed: 12946880]

Pinault D (2004). The thalamic reticular nucleus: structure, function and concept. Brain Res. Brain Res. Rev 46, 1–31. [PubMed: 15297152]

Pinault D, and Deschênes M (1998). Projection and innervation patterns of individual thalamic reticular axons in the thalamus of the adult rat: a three-dimensional, graphic, and morphometric analysis. J. Comp. Neurol 391, 180–203. [PubMed: 9518268]

Quirk GJ, Armony JL, and LeDoux JE (1997). Fear conditioning enhances different temporal components of tone-evoked spike trains in auditory cortex and lateral amygdala. Neuron 19, 613–624. [PubMed: 9331352]

Resnik J, and Paz R (2015). Fear generalization in the primate amygdala. Nat. Neurosci 18, 188–190. [PubMed: 25531573]

Resnik J, Sobel N, and Paz R (2011). Auditory aversive learning increases discrimination thresholds. Nat. Neurosci. 14, 791–796. [PubMed: 21552275]

Romanski LM, and LeDoux JE (1992). Equipotentiality of thalamo-amygdala and thalamo-cortico-amygdala circuits in auditory fear conditioning. J. Neurosci 12, 4501–4509. [PubMed: 1331362]

Romanski LM, Clugnet MC, Bordi F, and LeDoux JE (1993). Somatosensory and Auditory Convergence in the Lateral Nucleus of the Amygdala. Behav. Neurosci 107, 444–450. [PubMed: 8329134]

Sacco T, and Sacchetti B (2010). Role of secondary sensory cortices in emotional memory storage and retrieval in rats. Science 329, 649–656. [PubMed: 20689011]

Shosaku A (1986). Cross-correlation analysis of a recurrent inhibitory circuit in the rat thalamus. J. Neurophysiol 55, 1030–1043. [PubMed: 3711965]

Steriade M, Deschênes M, Domich L, and Mulle C (1985). Abolition of spindle oscillations in thalamic neurons disconnected from nucleus reticularis thalami. J. Neurophysiol 54, 1473–1497. [PubMed: 4087044]

Traub RD, Buhl EH, Gloveli T, and Whittington MA (2003). Fast rhythmic bursting can be induced in layer 2/3 cortical neurons by enhancing persistent Na+ conductance or by blocking BK channels. J. Neurophysiol 89, 909–921. [PubMed: 12574468]

Traub RD, Contreras D, Cunningham MO, Murray H, LeBeau FE, Roopun A, Bibbig A, Wilent WB, Higley MJ, and Whittington MA (2005). Single-column thalamocortical network model exhibiting gamma oscillations, sleep spindles, and epileptogenic bursts. J. Neurophysiol 93, 2194–2232. [PubMed: 15525801]

Traub RD, Contreras D, Cunningham MO, Murray H, LeBeau FE, Roopun A, Bibbig A, Wilent WB, Higley MJ, and Whittington MA (2005a). Single-column thalamocortical network model exhibiting gamma oscillations, sleep spindles, and epileptogenic bursts. J. Neurophysiol 93, 2194–2232. [PubMed: 15525801]

Traub RD, Contreras D, and Whittington MA (2005b). Combined experimental/simulation studies of cellular and network mechanisms of epileptogenesis in vitro and in vivo. J. Clin. Neurophysiol 22, 330–342. [PubMed: 16357637]

Villa AEP (1990). Physiological differentiation within the auditory part of the thalamic reticular nucleus of the cat. Brain Res. Brain Res. Rev 15, 25–40. [PubMed: 2364220]

Weinberger NM (2004). Specific long-term memory traces in primary auditory cortex. Nat. Rev. Neurosci 5, 279–290. [PubMed: 15034553]

Weinberger NM, Javid R, and Lepan B (1993). Long-term retention of learning-induced receptive-field plasticity in the auditory cortex. Proc. Natl. Acad. Sci. USA 90, 2394–2398. [PubMed: 8460150]

Willis AM, Slater BJ, Gribkova ED, and Llano DA (2015). Open-loop organization of thalamic reticular nucleus and dorsal thalamus: a computational model. J. Neurophysiol 114, 2353–2367. [PubMed: 26289472]

Wimmer RD, Schmitt LI, Davidson TJ, Nakajima M, Deisseroth K, and Halassa MM (2015). Thalamic control of sensory selection in divided attention. Nature 526, 705–709. [PubMed: 26503050]

Wood KC, Blackwell JM, and Geffen MN (2017). Cortical inhibitory interneurons control sensory processing. Curr. Opin. Neurbiol 46, 200–207.

Yang Y, Liu D-QQ, Huang W, Deng J, Sun Y, Zuo Y, and Poo M-MM (2016). Selective synaptic remodeling of amygdalocortical connections associated with fear memory. Nat. Neurosci 19, 1348–1355. [PubMed: 27595384]

Young A, and Wimmer RD (2017). Implications for the thalamic reticular nucleus in impaired attention and sleep in schizophrenia. Schizophr. Res 180, 44–47. [PubMed: 27510855]

Yukie M (2002). Connections between the amygdala and auditory cortical areas in the macaque monkey. Neurosci. Res 42, 219–229. [PubMed: 11900831]

Zikopoulos B, and Barbas H (2012). Pathways for emotions and attention converge on the thalamic reticular nucleus in primates. J. Neurosci 32, 5338–5350. [PubMed: 22496579]

Znamenskiy P, and Zador AM (2013). Corticostriatal neurons in auditory cortex drive decisions during auditory discrimination. Nature 497, 482–485. [PubMed: 23636333]

Highlights

- Basolateral amygdala projects to the TRN gating signals to the cortex
- BLA-TRN activation amplifies sound responses in the auditory thalamus and cortex
- A model for the BLA-TRN-AC connectivity explains the results
- This pathway is a potential target for treatment of emotional and sensory disorders

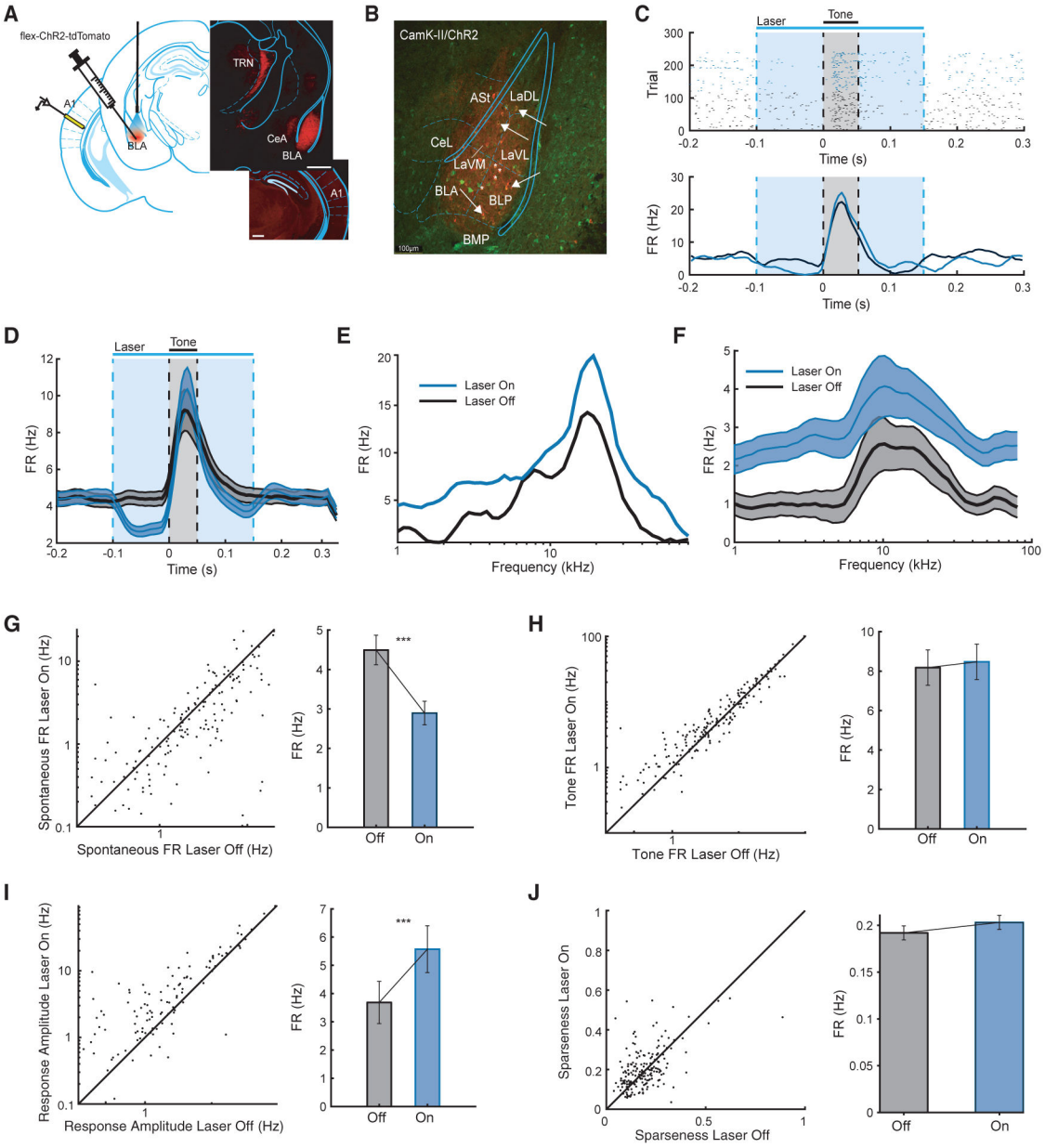

Figure 1. Photo-Activation of the BLA Increases Tone-Evoked Responses in the AC

(A) Left panel: CamK-cre mice were injected bilaterally with AAV-FLEX-ChR2-tdTomato into the BLA. Animals were implanted with optical fibers bilaterally targeting the BLA. Putative excitatory neurons in the BLA were activated by blue light (473 nm) while neuronal activity in the AC was recorded using either a multi-tetrode micro-drive or a multichannel silicon probe. Right panel: (Top) Micrograph showing expression of the injected virus in the BLA and its projections to the thalamus. (Bottom) Micrograph showing little labeling in the AC. Scale bar, 0.5 mm. AC, primary auditory cortex; BLA, basolateral amygdala; CeA, central nucleus of amygdala; TRN, thalamic reticular nucleus.

(B) Immunohistochemistry demonstrating the co-expression of ChR2-tdTomato in putative excitatory neurons in the BLA of a CamKIIα-Cre mouse. Red: tdTomato. Green: antibody for CamKIIα. Scale bar, 100 μm.

(C) Responses of a representative AC neuron to optogenetic stimulation of the BLA. Light was presented 100 ms prior to tone onset and continued for 100 ms after tone offset (−0.1 to 0.15 s [blue rectangle]). Tone was presented from 0 to 0.05 s (gray rectangle). Top: raster plot of spike times. Bottom: corresponding peristimulus time histogram (PSTH) of the neuronal response in light-on (blue) and light-off (black) conditions.

(D) PSTH of the AC neurons in response to a tone (gray rectangle) during light-on (blue line) and light-off (black line) trials. Time of photo-activation of the BLA is outlined by a blue rectangle. Plot shows data from all recorded AC neurons (N = 190 single units) from seven mice. Mean ± SEM.

(E and F) Frequency response function of the neuron from (B) (E) and mean frequency response function (F) in the absence of photostimulation (off trials) and during photostimulation of BLA (on trials).

(G–J) Optogenetic activation of BLA suppressed spontaneous firing rate (FR_{base}, G, paired t test, $t_{189} = 5.10$, p = 8.15e-7), but not tone-evoked activity of neurons recorded from AC (FR_{tone}, H, paired t test, n.s.). Therefore, the amplitude of tone-evoked response was increased (I, paired t test, $t_{189} = 6.72$, p = 2.12e-10). Activation of BLA did not affect sparseness of tuning of neurons in AC (J, paired t test, n.s.). Left panel: scatter plot of firing rate (G–I) or sparseness (J) on light-on plotted versus light-off trials. Each circle represents a single unit (red) or multi-unit (black). Right panel: mean ± SEM of measures from the left panel. ***p < 0.001 (paired t test).

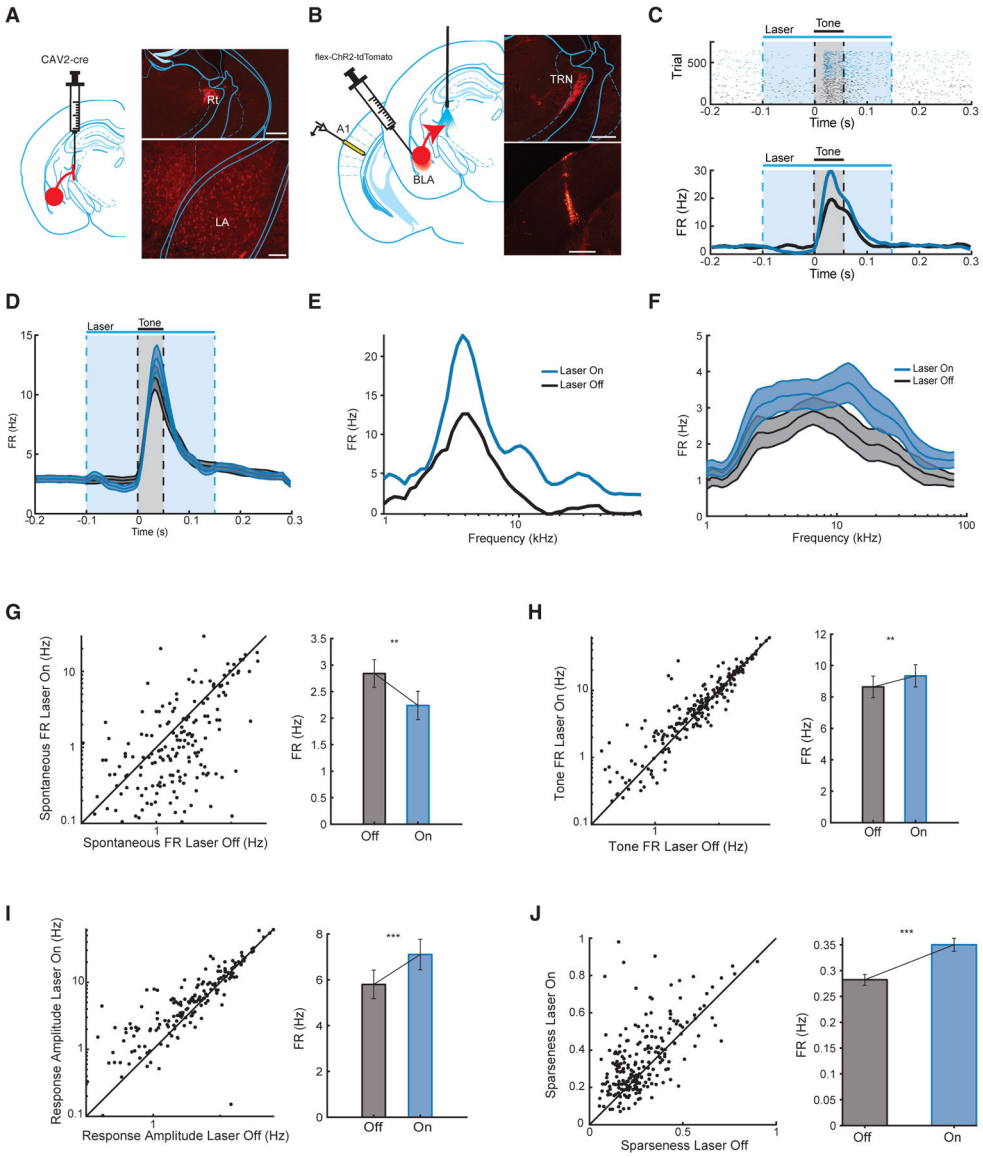

Figure 2. Photo-Activation of Projections from the BLA to the TRN Increases the Amplitude of Tone-Evoked Responses in the AC

(A) Left panel: retrograde tracing of the BLA projections to the TRN. AI14 mice were injected with CAV2-cre in the TRN. Right panel: (Top) micrograph showing the expression at the viral injection site in the TRN. Scale bar, 0.5 mm. (Bottom) Retrograde expression of tdTomato in neurons in the BLA and CeA. Scale bar, 0.1 mm.

(B) Anterograde tracing of the BLA projections to the TRN. Left panel: mice were injected bilaterally with the virus expressing ChR2 into the BLA. Animals were implanted with optical fibers bilaterally targeting the TRN. BLA-TRN projections were activated by blue light (473 nm) on the TRN while neuronal activity in the AC was recorded using a multichannel silicon probe. Right panel: (Top) micrograph showing projections in the TRN. (Bottom) Fluorescent trace from recording silicon probe. Scale bar, 0.5 mm.

(C) Responses of a representative AC neuron to the optogenetic stimulation of the TRN. Light was presented 100 ms prior to tone onset and continued for 100 ms after tone offset

(−0.1 to 0.15 s [blue rectangle]). Tone was presented from 0 to 0.05 s (gray rectangle). Top: raster plot of spike times. Bottom: corresponding PSTH of the neuronal response in light-on (blue) and light-off (black) conditions.

(D) Mean PSTH of the AC neurons in response to a tone (gray rectangle) in light-on (blue line) and light-off (black line) trials. Time of photo-activation of the TRN is outlined by a blue rectangle. Plot shows data from all recorded AC neurons (N = 216) from five mice. Mean ± SEM.

(E and F) Frequency response function of a representative neuron (E) and mean frequency response function (F) in the absence of photostimulation (off trials) and during photostimulation of the TRN (on trials).

(G–J) Optogenetic activation of the BLA-TRN projections suppressed the spontaneous firing rate (G) (FR_{base}, paired t test, $t_{215} = 2.74$, $p = 0.0067$), but increased the tone-evoked activity of neurons recorded from the AC (H) (FR_{tone}, paired t test, $t_{215} = 2.85$, $p = 0.0048$). Amplitude of the tone-evoked response was increased (I) (paired t test, $t_{215} = 5.65$, $p = 5.0e–8$). Activation of the BLA-TRN projections did not affect the sparseness of the tuning of neurons in the AC (J) (paired t test, $t_{215} = 6.62$, $p = 2.73e–10$). Left panel: scatterplot of firing rate (G–I) or sparseness (J) on light-on plotted versus light-off trials. Each circle represents a single unit. Right panel: mean ± SEM of measurements from the left panel. ***$p < 0.001$ (paired t test).

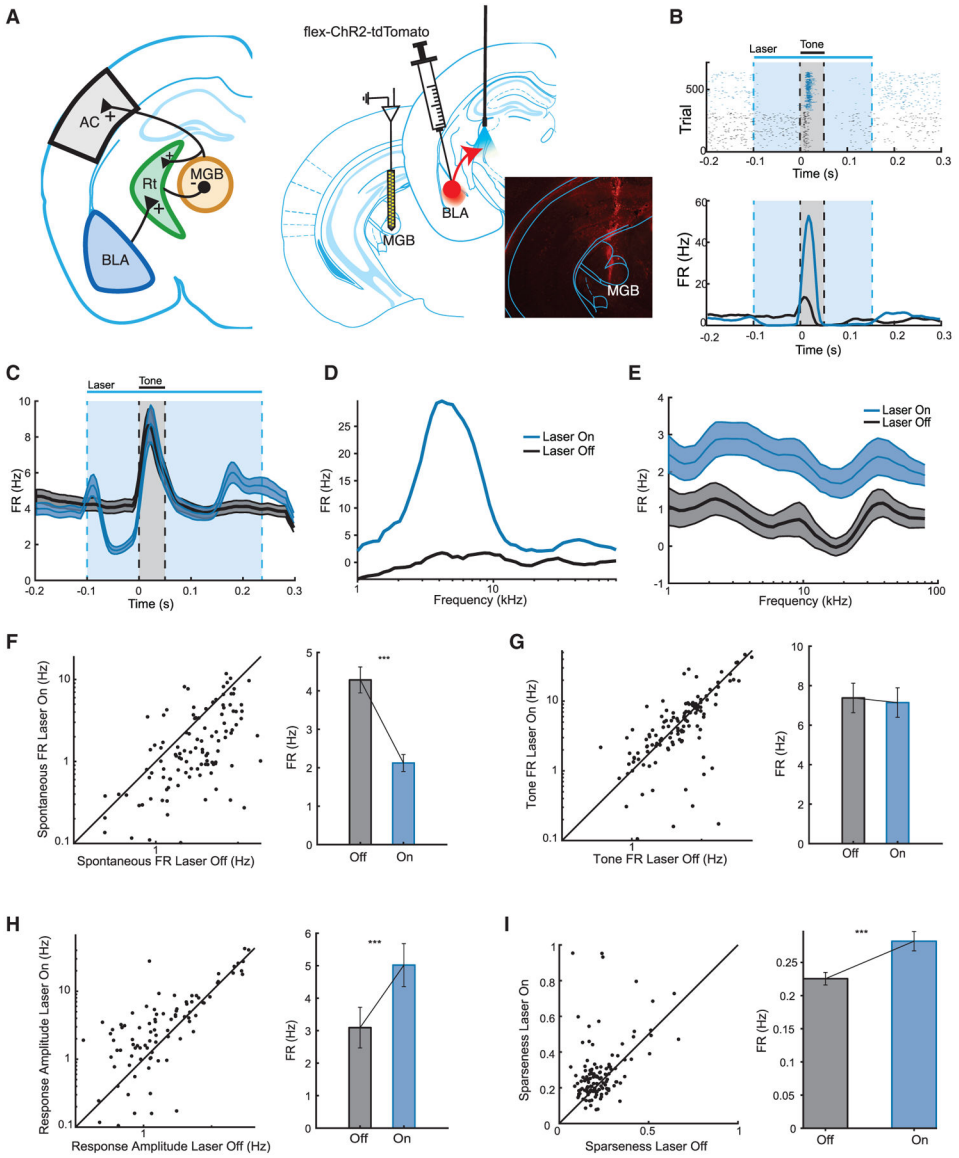

Figure 3. Photo-Activation of Projections from the BLA to the TRN Increases the Amplitude of the Tone-Evoked Responses in the MGB

(A) Left: diagram showing the proposed circuit underlying the effects of the amygdala-TRN pathway on auditory processing. Photo-activation of BLA-TRN projections ("+" synapses onto the TRN) leads to the inhibition of spontaneous activity and the amplification of the amplitude of tone-evoked activity of the MGB neurons as result of inhibition from the TRN ("−" synapses onto the MGB). This, in turn, amplifies auditory responses in the AC ("+" synapses onto AC). Right: (Left panel) mice were injected bilaterally with a virus expressing ChR2 into the BLA. Animals were implanted with optical fibers bilaterally targeting the TRN. BLA-TRN projections were activated by a blue light (473 nm) while neuronal activity in the MGB was recorded using a multichannel silicon probe. (Right panel) Micrograph showing fluorescent trace from the recording silicon probe. Scale bar, 0.5 mm.

(B) Responses of a representative MGB neuron to optogenetic stimulation of the TRN. Light was presented 100 ms prior to tone onset and continued 100 ms after tone offset (−0.1 to

0.15 s [blue rectangle]). Tone was presented from 0 to 0.05 s (gray rectangle). Top: raster plot of spike times. Bottom: corresponding PSTH of neuronal response in light-on (blue) and light-off (black) conditions.

(C) PSTH of the MGB neurons in response to a tone (gray rectangle) during light-on (blue line) and light-off (black line) trials. Time of photo-activation of the TRN is outlined by a blue rectangle. Plot shows data from all recorded MGB neurons (N = 126) from five mice. Mean ± SEM.

(D) Frequency response function of the neuron from (B) in the absence of photostimulation (off trials) and during photostimulation of the TRN (on trials).

(E) Mean frequency response functions of neurons from (C) in the absence of photostimulation (off trials) and during photostimulation of the TRN (on trials).

(F–I) Optogenetic activation of the BLA-TRN projections suppressed the spontaneous firing rate (F) (FR_{base}, paired t test, $t_{125} = 5.1$, $p = 8.97e{-}10$), but did not significantly change the tone-evoked activity of neurons recorded from the MGB (G) (FR_{tone}, paired t test, n.s.). The amplitude of the tone-evoked response was increased (H) (paired t test, $t_{125} = 5.16$, $p = 9.6e{-}7$). Activation of the BLA-TRN projections increased the sparseness of the tuning of neurons in the MGB (I) (paired t test, $t_{125} = 4.06$, $p = 8.65e{-}5$). Left panel: scatterplot of firing rate (F–H) or sparseness (I) on light-on plotted versus light-off trials. Each circle represents a single unit. Right panel: mean ± SEM of measures from the left panel. ***$p < 0.001$ (paired t test).

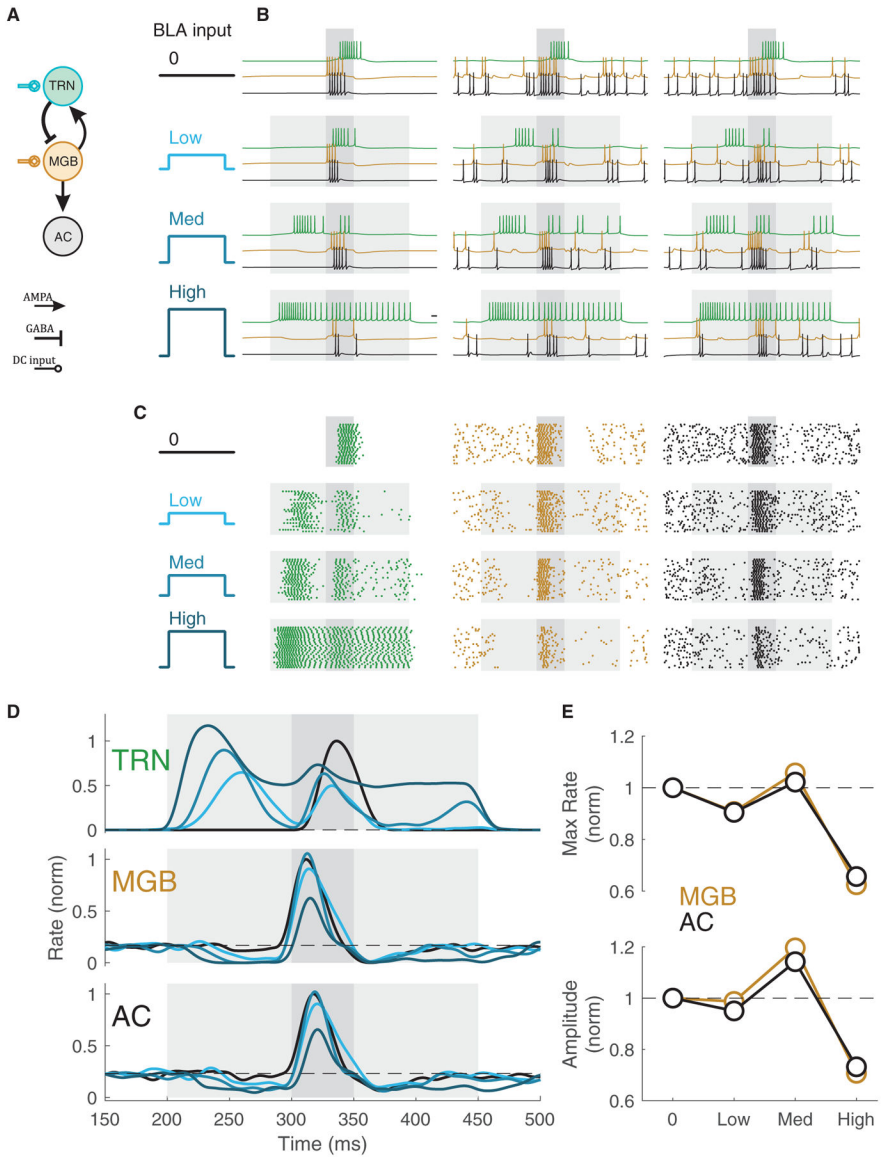

Figure 4. Possible Mechanism for BLA Enhancement of Tone-Evoked MGB and AC Responses

(A) Simulated network, including TRN, MGB, and AC cells (see Method Details). A 100-ms input to the TRN represented the optogenetic activation of the BLA. The tone was a 10-ms pulse to the MGB during the light stimulus.

(B) Simulations of the network for no spontaneous inputs (left column) and for two simulations with spontaneous input to the MGB and AC (middle and right columns), in the absence of BLA activation (top row) and with increasing strengths of BLA activation (lower rows).

(C) Spike rasters for 25 repeated simulations in (B).

(D) Spiking rates in the TRN, MGB, and AC neurons, shown for control conditions (black) and for the three strengths of BLA activation of the TRN (shades of blue), each normalized to zero-input values.

(E) Maximum firing rates in the MGB and AC during the tone (top), and peak-to-peak amplitudes of the tone response (bottom) shown for the varied strengths of BLA activation.

KEY RESOURCES TABLE

REAGENT or RESOURCE	SOURCE	IDENTIFIER
Antibodies		
Anti-CaMKII alpha Rabbit polyclonal (phospho T286) antibody	Abcam	Cat#: ab5683; RRID: AB_305050
Alexa 488 goat anti-rabbit IgG	Abcam	Cat#: ab150077; RRID: AB_2630356
Deposited Data		
Metadata for figures	This paper (Figures 1, 2, and 3)	https://doi.org/10.6084/m9.figshare.8226329
Data for Model (Figure 4)	This paper (Figure 4)	https://github.com/jhaaslab/trn_aud
Experimental Models: Organisms/Strains		
CamKIIα-Cre	Jackson Laboratories	B6.Cg-Tg(CamKIIα-Cre)T29-1Stl/J
AI14 reporter mice:	Jackson Laboratories	Rosa-CAG-LSL-tdTomato-WPRE::deltaNeo
Wild type	Jackson Laboratories	C57BL/6J; RRID: IMSR_JAX:000664
Recombinant DNA		
AAV9-FLEX-ChR2- tdTomato vector	Penn VectorCore	Addgene: 18917-AAV9; RRID: Addgene_18917
AAV5-CAG-hChR2(H134R)-mCherry-WPRE-SV40 vector	Penn VectorCore	Addgene: 100054-AAV5; RRID: Addgene_100054
Cav2-cre vector	Penn VectorCore	Viral Vector Production Unit
Software and Algorithms		
MATLAB	Mathworks	Mathworks.com; RRID: SCR_001622
ImageJ	NIH	https://imagej.nih.gov/ij/; RRID: SCR_003070
NEURON implementation in ModelDB	Traub et al., 2003, 2005; accession numbers 20756, 45539	accession numbers 20756, 45539